XVIII IMEKO WORLD CONGRESS
Metrology for a Sustainable Development
September, 17 – 22, 2006, Rio de Janeiro, Brazil

FEATURE EXTRACTION OF ONE PORT SCATTERING PARAMETERS FOR SINGLE ENDED LINE TESTING

Carine Neus [1], *Patrick Boets* [2], *Leo Van Biesen* [3]

[1] Vrije Universiteit Brussel, Brussels, Belgium, cneus@vub.ac.be
[2] Vrije Universiteit Brussel, Brussels, Belgium, pboets@vub.ac.be
[3] Vrije Universiteit Brussel, Brussels, Belgium, lvbiesen@vub.ac.be

Abstract: In order to identify if a subscriber loop is suitable for DSL service, the transfer function of the loop has to be estimated. Several measurement techniques exist, however Single Ended Line Testing is gaining much attention lately. This method allows only measuring at the central office side and yields a reflectogram. One of the critical issues in the estimation of the transfer function from this data is the correct extraction of the features of the reflectogram. This paper presents a new feature extraction algorithm for a previously reported transfer function estimator. It starts by explaining the previously reported algorithm. Its main drawbacks are modelling errors and loss of information due to the iterative approach. The paper explains how the new algorithm tackles these problems. The new method strongly relies of the first and second derivatives of the reflectogram, which is a completely new approach. Finally, the efficiency of both algorithms is compared. The improvements are both in terms of accuracy and identification time.

Keywords: Digital Subscriber Line (DSL), Single Ended Line Testing (SELT), loop qualification, feature extraction, transfer function estimation.

1. INTRODUCTION

When a customer asks for a certain DSL service, the first thing the operator needs to do, is verify whether this telephone line can support this service. This is called loop qualification and is different for each customer since it depends on the cabling between the customer premise (CP) and the central office (CO). By fixing the transfer function, the make-up of this subscriber loop will limit the maximum achievable bit rate and thus the possibility to support a certain service. Many topologies are possible, but typically a subscriber loop consists of several cable sections, possibly with a different diameter, spliced to each other, connecting the CP to the CO. Figure 1 gives an overview of the topologies considered in this paper.

The final channel capacity does not solely depend on the loop make-up, but also on the noise power spectral density (PSD) at both ends. However, the latter is not considered here and we will assume that correct loop topology estimation leads to correct loop qualification. Inaccurate loop estimation may lead to an overestimation of the achievable bit rate, resulting in customer dissatisfaction, or an underestimation of the achievable bit rate, resulting in loss of revenues. Hence, the accurate estimation of the loop is very important and the best way of qualifying a loop for DSL service is to test it.

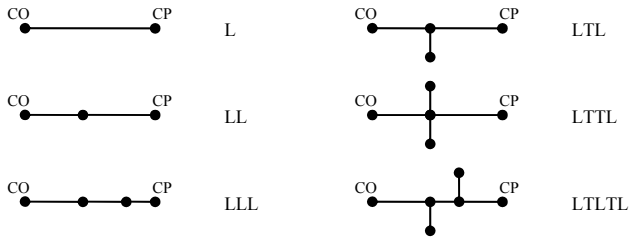

Figure 1 Supported topologies

Nowadays, commercial available instrumentation is based on Double Ended Line Testing (DELT). It requires a technician at both line extremities in order to quantify the loop transfer function. The determination of the subscriber loop in this way is expensive and requires the cooperation of the customer. Recently, the focus shifted to Single Ended Line Testing (SELT). With SELT, measurements are only performed at the CO side, which eliminates the necessity of dispatching a technician to the CP for each qualification. Therefore, SELT is often preferred by the telecom operators. However, in contrast to DELT, the loop transfer function cannot be measured directly from SELT data. The only measurable SELT quantity is the one-port scattering parameter, which is the ratio of the reflected to the injected wave [1]. Thus the loop make-up, from which we can calculate the transfer function, has to be extracted from this scattering parameter by advanced signal processing techniques.

For this we will use general knowledge of reflectometry. When exciting the network at the CO, the signal propagates on the line and whenever an impedance discontinuity is encountered, a reflection occurs and travels back to the measuring instrument. The reflection coefficient is given by (1) where Z_1 and Z_2 are the characteristic impedances of the lines before and after the discontinuity, respectively.

$$\rho = \frac{Z_2 - Z_1}{Z_2 + Z_1} \tag{1}$$

Collecting these reflections and plotting them over time, yields a reflectogram. For example an open line end will give a strong positive reflection ($Z_2 = \infty$), whereas a splice from a thinner to a thicker cable will give a negative reflection ($Z_2 < Z_1$). Figure 2 gives an example of such reflections. By determining the start time of a peak (Δt) it is possible to locate the line length l with formula (2) if the velocity of propagation v is known a priori.

$$l = \frac{v.\Delta t}{2} \qquad (2)$$

By analyzing the reflectogram, the line topology and thus also the loop transfer function, can be deduced [2]. Such a loop topology estimator was previously reported in [1]. It is important to mention that physical cable models are used rather than a black box model. Other approaches, like neural networks or models with lots of parameters are also possible but lack physical meaning. Unfortunately the feature extraction algorithm was limiting the overall accuracy of the estimator. Therefore a completely new algorithm is proposed in this paper, which is based on the derivatives of the reflectogram instead of relying on modelling and iteration.

The remainder of this paper is organized as follows. In Section 2, the complete model of the previously reported loop topology estimator is explained and the feature extraction is situated. In Section 3 we first describe the original feature extraction algorithm and its drawbacks. Then we propose a new algorithm and we explain how these specific problems are tackled. In Section 4, we demonstrate the performance enhancement. Section 5 summarizes the most important conclusions.

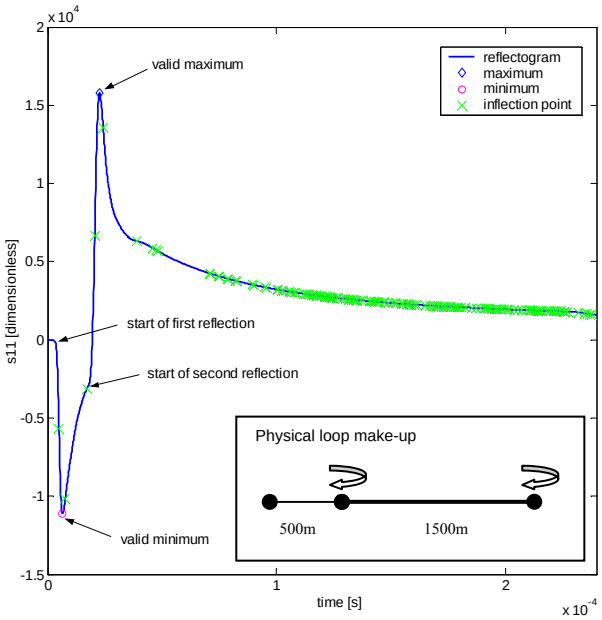

Figure 2 Reflectogram with maxima, minima and inflection points indicated for a 500 m segment (0.4 mm diameter) in series with a 1500 m segment (0.6 mm diameter)

2. DESCRIPTION OF THE MODEL

The complete model of the loop topology estimator is depicted in Figure 3. First, the one-port scattering parameter $S_{11}(\omega)$, which is the ratio of the reflected wave to the incident wave, is measured by means of a network analyzer directly in the frequency domain using sine waves as excitation signals [1]. The pre-processing will transform the obtained scattering parameter $S_{11}(\omega)$ into its time domain counterpart $s_{11}(t)$, the so-called reflectogram. Several pre-processing operations are necessary to visualize the reflection information in the reflectogram as explained in [3]. Once the pre-processor conditioned the reflectogram, the most important characteristics of $s_{11}(t)$, called 'features' can be detected (e.g. the start of a reflection). The feature extraction is the subject of this paper and will be discussed in more detail in Section 3.

Once the features of $s_{11}(t)$ are defined, a probabilistic reasoning system, called belief network, uses them to deduce the probability distribution function (pdf) over the supported loop topologies shown in Figure 1. Then a deterministic Rule Based System reasons further to confirm the most probable topology proposed by the Belief Network and determines the delay of each line section. If the proposed topology produces inconsistent results, the second most probable topology is investigated, and so on. Finally a last module fine-tunes the values of the line segments by minimizing a cost function and produces the estimated subscriber loop topology [4].

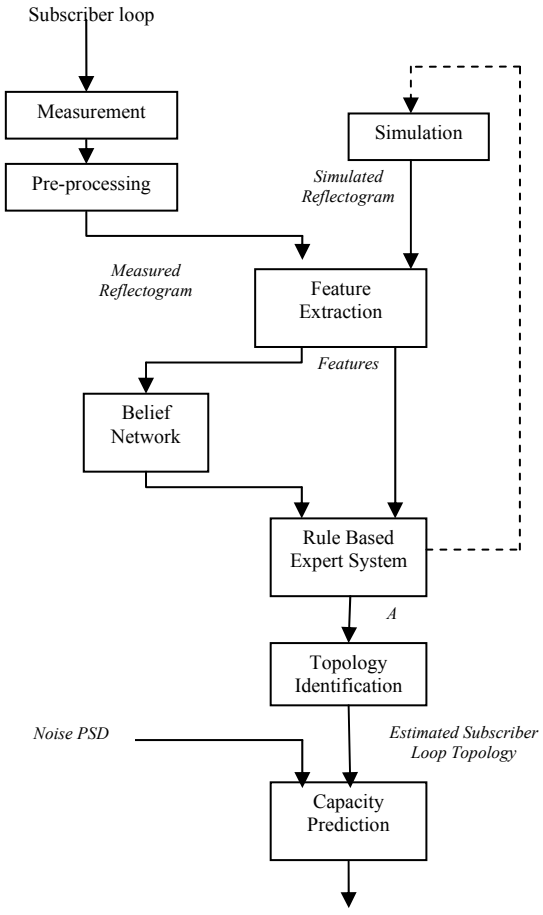

Figure 3 Model of the loop topology estimator

At this point, the loop topology has been derived from the SELT measurement and hence the loop transfer function can be computed. If the PSD of the noise at the CO and at the CP is known, using a direct measurement or a model-based estimation, then a bit rate prediction is possible.

3. FEATURE EXTRACTION

The feature extraction analyzes the reflectogram in order to extract the features, being the number of peaks and their attributes visible in the signal. These peaks correspond to reflected pulses travelling back to the CO due to impedance discontinuities. Important attributes are the start and the end of each observed reflection, the position of the extremum and the type of extremum (maximum or minimum).

The feature extraction's task is to decompose the reflectogram, which represents the sum of all the reflections, to a series of non-interfering reflections. This is necessary because each k-th peak p_k is superimposed on the tail of the preceding peaks p_{k-1}, p_{k-2},…, p_1, therefore distorting the isolated shape of the individual peaks.

3.1. Drawbacks of the original algorithm

In the original implementation of the feature extraction [5], each detected peak was decoupled from the previous peaks by applying the following steps. First the features $(n_{start,k}, n_{extremum,k}, n_{end,k})$ of the peak p_k were detected where n denotes the index. Next a numerical prediction of the tail t_{p_k} was done in the interval $[n_{extremum,k}, n_{end,k}]$. Two models for t_{p_k} are distinguished:

$$t_{p_k}(n) = e^{an+b} \tag{3}$$

$$t_{p_k}(n) = \frac{1}{an+b} \tag{4}$$

The prediction of $p_k(n)$ is then defined as :

$$\tilde{p}_k(n) = \begin{cases} s_{11,k}(n) & n < n_{end,k} \\ t_{p_k}(n) & n \geq n_{end,k} \end{cases} \tag{5}$$

In Figure 4 an example is given of such a prediction. The third step is the subtraction of the predicted peak $\tilde{p}_k(n)$ from $s_{11,k}(n)$, yielding a residue signal. These three steps are applied iteratively to the residue signal until no new peaks are detected or the energy in $s_{11,k}(n)$ is below a certain threshold. The end result is a list of detected peaks.

This method has two main drawbacks. Firstly, modelling errors are inevitable. The models (3) and (4) are workable tail models in practice. However, when the loop topology is complex or when the fit interval is too short, these modelling errors can cause false peaks to appear. Secondly, when three consecutive reflections occur, often only two are detected. We will discuss Figure 4 to illustrate this problem.

The first reflection is due to the splice of the first two line segments and is negative because the second line segment has a larger diameter and thus has a smaller characteristic impedance, resulting in a negative reflection coefficient [6]. For the same reason, the second reflection is

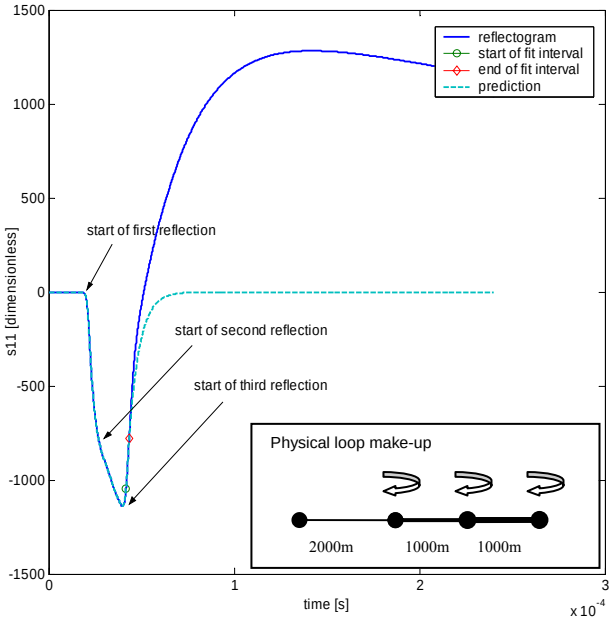

Figure 4 First predicted tail of a reflectogram for a 2000 m segment (0.4 mm diameter) in series with 1000 m (0.6 mm diameter) and 1000 m (0.8 mm diameter)

negative as well. The third reflection is due to the line end after a total of 4 km and is positive due to the infinite impedance of the load ('open'). As one can see from Figure 4 the first two negative reflections are merged. For clarity, the start of each reflection is indicated on Figure 4, although the algorithm does not detect the start of the second reflection.

After determining the features of the first peak, the predicted peak is subtracted and the algorithm starts again with the residue signal. Since the amplitude of prediction is everywhere equal to or lower than the amplitude of the reflectogram, the residue signal will be completely positive. At this point, the second negative peak can never be recovered. Only the first negative and the last positive peak are detected. Thus, with the existing algorithm, when two consecutive reflections cause two peaks to merge, resulting in only one extremum instead of two, one peak is left undetected. This problem is not to be neglected, since it happens quite often for topologies with more than two line segments, especially when the second line segment is short compared to the first one.

3.2. New feature extraction algorithm

Since the original feature extraction technique has serious problems inherent to the followed approach, in the remainder of this paper, a completely new approach is presented. Here, no modelling of the tails is done and iteration is avoided. Instead, the superposition of the peaks is left unaltered and all the features are detected in one pass. How the individual peaks can be recovered with this new method, is illustrated in the following example.

In Figure 2, the first reflection was negative and was due to the splice of the two line segments. The second reflection was due to the line end after a total of 2 km and was positive. It can be seen that the second reflection is superimposed on the tail of the first reflection because the

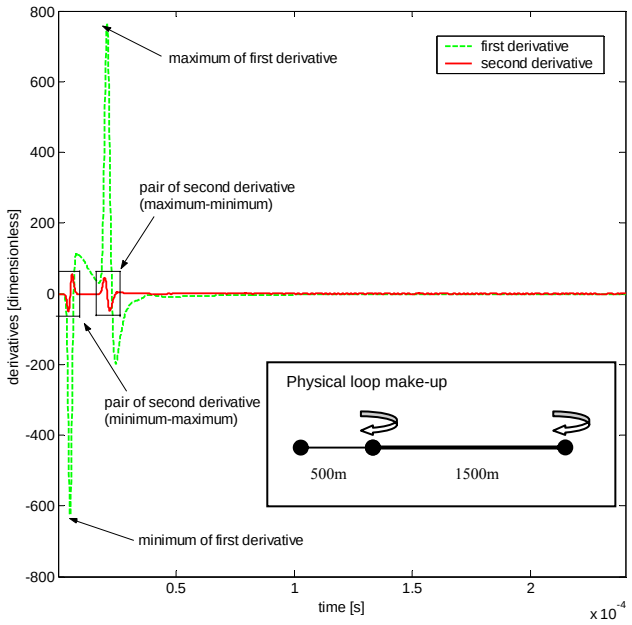

Figure 5 First and second derivative of the reflectogram depicted in Figure 2

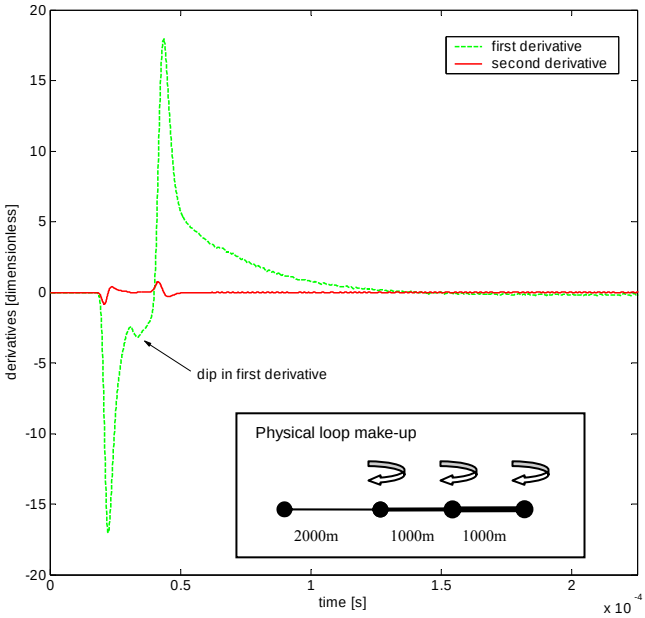

Figure 6 First and second derivative of the reflectogram depicted in Figure 4

second reflection arrives while the tail of the first reflection is not yet completely extinct. Figure 5 shows the first and the second derivatives of the reflectogram depicted in Figure 2. It can be seen that every minimum in the reflectogram (Figure 2) induces a minimum of the first derivative (Figure 5) as well as a 'pair' in the second derivative (a minimum followed by a maximum). Similarly, every maximum in the reflectogram induces a maximum in the first derivative and a 'pair' of the second derivative (a maximum followed by a minimum).

The new implementation of the feature extraction is based on these pairs of the second derivative. The algorithm searches for valid pairs in the second derivative. In order for a pair to be valid, several constraints are imposed on the values of the reflectogram, the first derivative and the second derivative. Basically, a minimum-maximum pair is only valid if:

- the pair has an amplitude above a certain threshold,
- the minimum and maximum have comparable amplitude,
- there is a corresponding minimum in the first derivative
- and the reflectogram is negative in this point.

For a maximum-minimum pair the conditions are less stringent, as there is no equivalent of the last condition. The first two conditions remain the same, while the third one requires a corresponding maximum in the first derivative.

Some exceptions to these rules are allowed in special cases. The operation of the new feature extraction is schematically shown in Figure 7. Each valid maximum-minimum pair in the second derivative indicates the start of a positive reflection. In a similar way, each valid minimum-maximum pair in the second derivative indicates the start of a negative reflection. More details can be found in [7].

In the presence of noise, the use of derivatives can sometimes be problematic. This is avoided here, since several measurements are performed in order to average out the noise influence. The first condition serves as an additional security that noise will not lead to the detection of false features.

In the difficult case of the situation depicted in Figure 4, the new algorithm will detect the three reflections because every start of a reflection induces a change in the slope of the reflectogram, inducing a pair in the second derivative. The dip in the first derivative clearly shows there is a change in the slope of the reflectogram (see Figure 6). The pair in the second derivative is also present, but cannot be seen on this scale. Since all conditions are fulfilled, the algorithm concludes that there is a second negative reflection starting at the beginning of the dip. The three reflections (2 negative, 1 positive) are correctly detected.

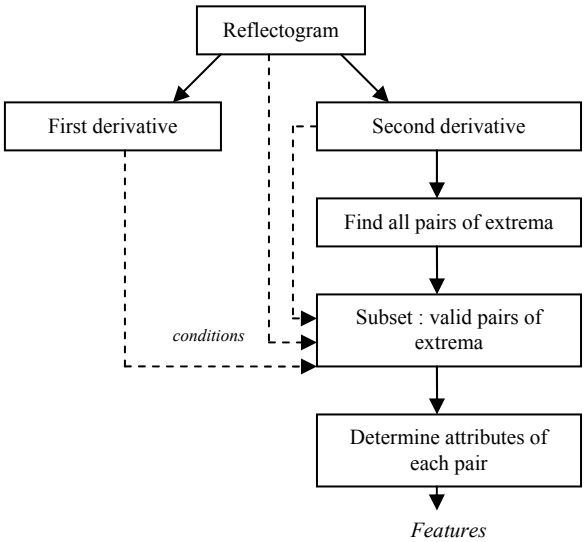

Figure 7 Schematic operation of the new feature extraction

4. SIMULATION RESULTS

In order to test the performance of the new feature extraction and as not enough reliable measurements were available, an extensive set of simulations has been created. Different combinations of lengths have been simulated for the topologies mentioned in Figure 1, with a total length limited to 4 km. The loop topology estimator (depicted in Figure 3) has processed all these simulations, once with the original feature extraction algorithm and once with the new one. We will compare the estimated loop topology before fine-tuning (point A in Figure 3), in order to see the effect of the new algorithm more clearly. At this point the Rule Based Expert System has decided which topology is most probable and has calculated the line lengths according to (2).

First of all, we calculate the number of correctly characterised topologies. As can be seen from Table 1 the new algorithm performs better for single line segments as well as for cascades of line segments. Especially with LLL-topologies, the probability of finding the correct topology is greatly increased. As explained in Section 3, the original algorithm had trouble correctly identifying topologies with merged reflections, which is often the case for topologies with three line segments. The new algorithm does not suffer from this problem and thus leads to an important increase in the number of correctly characterized LLL-topologies.

When both algorithms result in the correct topology, we can also compare the accuracy of the estimated cable lengths. We define the accuracy as

$$accuracy = \frac{|estimated\_length - real\_length|}{real\_length}.100\% \quad (6)$$

The accuracy of the L- and LL-topologies is comparable for both algorithms (over 90%). For the LLL-topologies, the accuracy of the estimated length of the first line segment is almost equivalent for both techniques, but the new approach greatly improves the accuracy of the estimated length of the second and third line segment and consequently of the total length (see Table 2). This comes from the fact that the starting point of the second reflection was sometimes very inaccurate with the original algorithm due to a poor fit. As the new algorithm determines the start of a reflection when a change in slope is noticed, the start of the reflection is more accurate. Consequently, the following segments are also more accurate. The first line segment was never a problem since at this point the original algorithm is in its first iteration and thus works with the original reflectogram.

The three last topologies consider the presence of a tap, which is a short piece of cable (typically not more than 500 m), connected in parallel and left unterminated. Taps are often placed when cabling a new neighbourhood in order to leave flexibility for future connections. In the presence of taps, again the topology is defined correctly more often (see Table 3). Table 4 compares the accuracy of the estimated lengths for the correctly estimated LTL case. Again, the new algorithm performs as good or better for all the individual lengths and also for the total length. The percentage of correctly characterized taps is however still unsatisfactory. The detection of taps is difficult because each tap causes two

Table 1 : Percentage of correctly characterized topologies

	Original	New
L-topologies (30 simulations)	90%	100%
LL-topologies (27 simulations)	85%	96%
LLL-topologies (56 simulations)	39%	82%

Table 2 : Accuracy of the estimated length for LLL-topologies

	Original	New
First line segment	76%	80%
Second line segment	77%	93%
Third line segment	78%	95%
Total line length	85%	98%

Table 3 : Percentage of correctly characterized topologies

	Original	New
LTL-topologies (81 simulations)	37%	65%
LTTL-topologies (160 simulations)	4%	26%
LTLTL-topologies (208 simulations)	16%	23%

Table 4 : Accuracy of the estimated length for LTL-topologies

	Original	New
First line segment	96%	97%
Second line segment	54%	70%
Tap length	48%	56%
Total line length	82%	84%

reflections: a first reflection at the parallel junction and a second at the tap end. This complicates the identification of topologies containing taps.

Another parameter that should be considered is the computational cost. It should be mentioned that neither of the two algorithms was optimised in this aspect. However, we expect the new algorithm to perform better for two reasons. Firstly, the feature extraction -in contrast to the original algorithm- is not iterative and secondly, no more modelling is involved. This expectation is confirmed in Figure 8. The mean time of the new algorithm is clearly lower than the mean time of the original one. Moreover, it

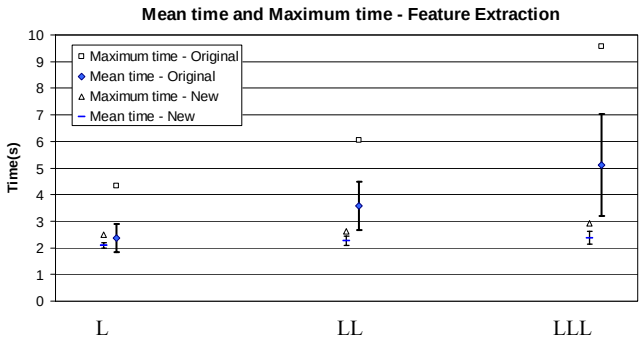

Figure 8 Mean time, maximum time and standard deviation for the Feature Extraction

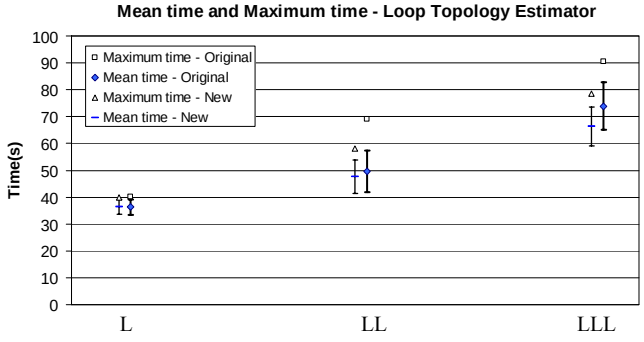

Figure 9 Mean time, maximum time and standard deviation for the loop topology estimator

has a lower standard deviation and a lower maximum error. But what is most important is the fact that the mean time is almost constant, independent of the topology, whereas the mean time of the original algorithm increased with the complexity of the topology.

Moreover, we expect the total execution time of the loop topology estimator to be lower because less peaks are left undetected, which simplifies the identification for the reasoning modules. Comparing the time gain of the feature extraction algorithm (Figure 8) to the time gain of the loop topology estimator (Figure 9) shows there is indeed also a time reduction in the reasoning modules.

5. CONCLUSION

This paper proposed a new feature extraction algorithm for a previously reported loop topology estimator. With the new feature extraction, the two main drawbacks of the original feature extraction, namely the modelling errors and the undetected peaks in the case of overlapping peaks are avoided. This results for all the supported topologies, in an important increase of correctly estimated loop topologies. Especially the topologies with more than two segments are classified correctly more often. Analysis showed that the accuracy of all the supported topologies is comparable or better. In addition, the execution time is lower. Finally, an improved feature extraction algorithm allows a more accurate estimation of the maximum achievable bit rate for DSL service.

If it is feasible to perform loop topology identification via single-ended measurements with sufficient accuracy, then operators will benefit substantially because, besides automatic qualification a loop for DSL service, this capability will allow the updating of telephone company loop make-up records. These records can in turn be accessed to facilitate engineering, provisioning and maintenance operations.

6. REFERENCES

[1] T. Bostoen, P. Boets, M. Zekri, L. Van Biesen, T. Pollet and D. Rabijns, “Estimation of the Transfer Function of a Subscriber Loop by Means of One-Port Scattering Parameter Measurement at the Central Office”, IEEE Journal on Selected Areas in Communication-Twisted Pair Transmission, Vol. 20, No. 5, pp936-948, June 2002

[2] S. Galli, D.L. Waring, “Loop Makeup Identification Via Single Ended Testing: Beyond Mere Loop Qualification”, IEEE Journal on Selected Areas in Communication-Twisted Pair Transmission, Vol. 20, No. 5, pp923-935, June 2002

[3] P. Boets, T. Bostoen, L. Van Biesen and T. Pollet, “Measurement, Calibration and Pre-Processing of Signals for Single-Ended Subscriber Line Identification”, Proceedings of the 20th IEEE Instrumentation and Measurement Technology Conference, 20-22 May, 2003

[4] P. Boets, T. Bostoen, D. Gardan, and L. Van Biesen, “Single-Ended Line Testing – A White Box Approach”, Proceeding of Wireless and Optimal Communication, Banff, Canada, 8-10 July, 2004

[5] T. Vermeiren, T. Bostoen, F. Louage, P. Boets, and X. O. Chebab, “Subscriber Loop Topology Classification by means of Time Domain Reflectometry”, IEEE International Conference on Communications, Anchorage USA, 11-15 May, 2003

[6] X. Ochoa Chehab, “Expert System for Automated TDR Interpretation using a Double Level Generate-Test-Debug Approach”, M.S. Thesis, Dept. ELEC, Vrije Universiteit Brussel, 2002

[7] C. Neus, “Feature Extraction of One Port Scattering Parameters for Single Ended Line Testing”, Master Thesis, Dept. ELEC, Vrije Universiteit Brussel, 2004